HOKKAIDO UNIVERSITY

Title	Phase space geometry of dynamics passing through saddle coupled with spatial rotation
Author(s)	Kawai, Shinnosuke; Komatsuzaki, Tamiki
Citation	Journal of Chemical Physics, 134(8), 084304 https://doi.org/10.1063/1.3554906
Issue Date	2011-02-28
Doc URL	https://hdl.handle.net/2115/45020
Rights	Copyright 2011 American Institute of Physics. This article may be downloaded for personal use only. Any other use requires prior permission of the author and the American Institute of Physics. The following article appeared in J. Chem. Phys. 134, 084304 (2011) and may be found at https://dx.doi.org/10.1063/1.3554906
Type	journal article
File Information	JCP134-8_084304.pdf

Hokkaido University Collection of Scholarly and Academic Papers : HUSCAP

Phase space geometry of dynamics passing through saddle coupled with spatial rotation

Shinnosuke Kawai[a),b)] and Tamiki Komatsuzaki
Molecule & Life Nonlinear Sciences Laboratory, Research Institute for Electronic Science, Hokkaido University, Kita 20 Nishi 10, Kita-ku, Sapporo 001-0020, Japan

(Received 5 December 2010; accepted 26 January 2011; published online 22 February 2011)

Nonlinear reaction dynamics through a rank-one saddle is investigated for many-particle system with spatial rotation. Based on the recently developed theories of the phase space geometry in the saddle region, we present a theoretical framework to incorporate the spatial rotation which is dynamically coupled with the internal vibrational motions through centrifugal and Coriolis interactions. As an illustrative simple example, we apply it to isomerization reaction of HCN with some nonzero total angular momenta. It is found that no-return transition state (TS) and a set of impenetrable reaction boundaries to separate the "past" and "future" of trajectories can be identified analytically under rovibrational couplings. The three components of the angular momentum are found to have distinct effects on the migration of the "anchor" of the TS and the reaction boundaries through rovibrational couplings and anharmonicities in vibrational degrees of freedom. This method provides new insights in understanding the origin of a wide class of reactions with nonzero angular momentum. © *2011 American Institute of Physics*. [doi:10.1063/1.3554906]

I. INTRODUCTION

Chemical reaction is a rearrangement of particles (atoms) constituting the system (molecule) which involves transition from one state (reactant) to another (product). In many reactions, there exists a rank-one saddle point on a single effective potential energy surface (typically, in a space of $3N-6$ dimension where N is the number of particles), nearby which the system passes from the reactant to the product. Recent theoretical developments on nonlinear dynamics through the saddle have revealed the robust existence of *no-return* transition state (TS) and the reaction pathway along which *all* reactive trajectories necessarily follow not in the *configuration* space but in the *phase* space. In addition to what chemists have long envisioned as TS,[1–8] it was revealed that there exist another important "building blocks" in the phase space for the understanding of the origin of the reactions: that is, normally hyperbolic invariant manifold (NHIM) and the stable/unstable invariant manifolds[9–17] (and their remnants[16,18–21]). An invariant manifold is a set of points in the phase space such that, once the system is in that manifold, the system will stay in it perpetually.

The most important invariant manifolds in reactions is those of codimension *one*, that is, the dimension of the manifold is *one* less than that of the phase space. Such a manifold can divide the space into two distinct regions [e.g., remember that a three-dimensional space can be divided by a two-dimensional space (e.g., sheet) but not by a one-dimensional space (line)]. Due to the invariance of the manifold, no trajectory can cross it from one side to the other in the phase space. The stable/unstable invariant manifolds emanating from the NHIM are of codimension one and separate the phase space into two distinct regions in which all the trajectories are led to either the state of the reactant or that of the product. Once we know which side of the manifold a given initial condition is, we can immediately know, without any trajectory calculations, whether the initial condition brings the system to the product or not. Note that the TS is also required to be of codimension one, otherwise one cannot identify "before" and "after" the reaction, corresponding to the states of reactant and products. The conventional TS defined by a constraint of $q_1 = 0$ by a certain "reaction coordinate" q_1 holds the correct dimensionality of the TS since the number of the constraint is just one (i.e., $q_1 = 0$), implying codimension one at constant energy, even if it may not resolve the nonrecrossing problem.

Thanks to normal form (NF) theories (a classical analog of quantum Van Vleck perturbation theory), it was revealed in classical Hamiltonian systems with many degrees of freedom,[9,10,17,19,22–38] that one can robustly extract the NHIM, no-return TS, and the stable/unstable invariant manifolds up to a moderately high energy regime above the saddle point energy, even under the existence of chaos arising from nonlinear couplings. The potential of the theories has been demonstrated not only in chemical reactions with[17,22] and without[23–27] time-dependent external field but also in ionization of a hydrogen atom in crossed electric and magnetic fields,[28–30] isomerization of clusters,[31–36] and the escape of asteroids from Mars[37,38] [Just recently the theory was also generalized to quantum Hamiltonian systems[39–41] and dissipative (generalized) Langevin systems.[42–51]]

The dimension of the phase space of an N-particle nonrigid system is $(6N-10)$ in the upper limit.[52] Nonrigid molecules at constant energy have ten constraints of the three coordinates of center of mass, the three conjugate momenta of center of mass, the three angular momenta (defined in the space-fixed frame), and the total energy of the system. If

[a)]Electronic mail: skawai@es.hokudai.ac.jp.
[b)]Research Fellow of the Japan Society for the Promotion of Science

 © 2011 American Institute of Physics

Downloaded 22 Mar 2011 to 133.87.26.199. Redistribution subject to AIP license or copyright; see http://jcp.aip.org/about/rights_and_permissions

nontrivial constant(s) of motion exist(s), the dimension of the phase space further decreases by the number of the nontrivial constant(s) of motion. Beck *et al.*[52] studied the change of dimensionality of the phase space in isomerization reaction of Ar_3 cluster as a function of the total energy of the system. It was found that the dimension of the phase space covers from three at very low energy regime where the systems are confined on high-dimensional torus to eight at very high energy of very nonrigid regime. They also found an intermediate energy regime of dimension five, where vibrational modes are coupled with each other but the system is regarded as still relatively rigid, so that the overall rotation in the space-fixed frame exhibits approximate three constants of the motion.

Although the dimension of the phase space of chemical reaction can be subject to not only vibrational degrees of freedom but also the overall rotation, most investigations of the phase space geometry of reaction dynamics have been focused on zero total angular momentum ($\mathbf{J} = \mathbf{0}$) case, except for the works by Wiesenfeld *et al.*[53,54] The difficulty comes from the fact that NF theory usually starts with harmonic approximation around a saddle point. The rotational motion is greatly different in its geometrical and algebraic structure from the harmonic vibration and the passage over the parabolic barrier on the potential. In reality many reactions can take place in a wide region of nonzero total angular momentum ($\mathbf{J} \neq \mathbf{0}$) in the **J**-space due to thermal excitation of unimolecular systems or nonzero impact parameter of bimolecular collisions. Note that $\mathbf{J} = \mathbf{0}$ is just a pinpoint in the **J**-space. In the studies of Wiesenfeld,[53,54] the concept of relative equilibrium (RE) has been introduced, which replaces the role of the saddle point in the rotationless case. Change of the position and the linear stability of RE was systematically investigated as a function of **J**. It was shown that the height and the position of RE move with the change of **J** resulting in a transition of reaction dynamics from chaos to regular in nature, and eventually to the cease of reaction. Time-reversal *a*symmetry of RE due to Coriolis interactions was also found. Unfortunately, their investigation was limited to planar systems. There we have only one component of the angular momentum **J**, which is a constant of motion. It can thus be treated like a constant parameter, leaving the system with the other degrees of freedom, which are vibrations and passage over an inverted parabola. In general, for spatial rotation, however, only the modulus $|\mathbf{J}|$ is constant whereas each component (J_a, J_b, J_c) in the body-fixed frame changes with time for asymmetric top molecules.

Compared to the rotational effects in the saddle region, rovibrational coupling in the potential well region has a long history of study. Clodius and Shirts[55] investigated the coupling between the two stretching modes of H_2O and D_2O rotating in a plane. Since there is only one component of angular momentum for planar rotation and it is conserved, the angular momentum acts as a constant parameter in the Hamiltonian. The coupling strength between the two stretching vibrations is thus changed with the change of the angular momentum. It was found that the increase of the angular momentum first decreases the chaotic behavior of the system for low J, and then increases the chaos for high J. This was successfully explained by the consideration of the sign of the coupling term and its dependence on J through the centrifugal term. Similarly, the change of the strength of coupling with the change of the angular momentum was found in the study of energy flow between two vibrational modes under the effect of Coriolis force.[56] There again the rotation was restricted to a plane and the angular momentum was a constant parameter to change the magnitude of vibrational coupling. In contrast to the planar rotation, inclusion of three-dimensional rotation can result in *energy exchange between rotation and vibration*.[57] Trajectories of triatomic molecules OCS and SO_2 were studied through Fourier transforms and rates of trajectory divergence. In the major part of the OCS trajectories, regular-type energy flow was observed through a 2:1 resonance between two frequencies of the bending normal mode and the rotation. In SO_2, the rovibrational coupling was more complex because all the vibrational modes are strongly coupled by anharmonicity and the trajectories showed chaotic behavior. In both cases, the energy exchange between rotation and vibration was dominated by the centrifugal term. The significance of 2:1 centrifugal resonance was later confirmed in the analyses with Poincaré surfaces of sections of a simplified model by Ezra,[58] where other resonances (4:1 and two 3:1's) were also found and closely analyzed. Another interesting phenomena found in these studies is the chaotic breakdown of the separatrix in the **J**-space and a transition over it. In the rigid rotor, there is a separatrix in the three-dimensional **J**-space (which will be explained in Sec. II B for the sake of completeness) that acts as an impenetrable separatrix to separate the rotational motion around the molecular A-axis and that around the C-axis. Under the existence of rovibrational resonance, the separatrix region becomes chaotic and some trajectories show transitions between A-type motion and C-type motion. The resonance structures and chaotic breakdown of separatrix were later analyzed by first-order classical perturbation theory.[59] While the separatrix and the stability of planar rotation are broken through chaos, there were found to be stabilizing resonances that generate motions different from the rigid rotor but still regular. In summary, the rotational motion can actively couple to the internal motion of molecules and significantly change it. Although the above researches were performed for vibrational motions in potential wells, it is expected that the rotation can also change actively the reaction dynamics in the saddle region. As a starting point, we investigate in the present paper an energy regime where the rovibrational coupling invalidates the normal mode description but the dynamics is still regular. Investigation of the above mentioned resonance structure and chaotic breakdown with similar methods would also be a fascinating subject in the future.

In this paper, we present a new framework based on NF theory with spatial rotation, in which (J_a, J_b, J_c) are explicitly treated as dynamical variables (in Sec. II). This incorporates the effects of nonlinear rovibrational couplings and enables us to extract the phase space reaction coordinate separated from the other (vibrational and rotational) modes. As an illustrative example, we apply the theory to HCN molecule in Sec. III. It is found that the NHIM (and hence the position of the no-return TS and the stable/unstable invariant manifolds)

Downloaded 22 Mar 2011 to 133.87.26.199. Redistribution subject to AIP license or copyright; see http://jcp.aip.org/about/rights_and_permissions

migrates with increasing J, to which the different components (J_a, J_b, J_c) have different effects. Summary and outlook will be given in Sec. IV.

II. THEORY

A. Setting of the problem

The Hamiltonian for the rovibrational motion of a molecule is given by[60]

$$H(\mathbf{J},\mathbf{q},\mathbf{p}) = \frac{1}{2}\left(\mathbf{J} - \sum_{k,k'} \boldsymbol{\zeta}_{k,k'} q_k p_{k'}\right)^{\mathrm{T}} \times \mathbf{M}(\mathbf{q}) \left(\mathbf{J} - \sum_{k,k'} \boldsymbol{\zeta}_{k,k'} q_k p_{k'}\right) + \frac{1}{2}\sum_k {p_k}^2 + V(\mathbf{q}), \tag{1}$$

$$\mathbf{M}(\mathbf{q}) = \left(\mathbf{I}(\mathbf{q}) - \sum_{k,k',k''} \boldsymbol{\zeta}_{k',k} q_{k'} \boldsymbol{\zeta}^{\mathrm{T}}_{k'',k} q_{k''}\right)^{-1}, \tag{2}$$

where $\mathbf{J} = (J_a, J_b, J_c)$ is the angular momentum projected onto the molecular axes(a, b, c), the matrix $\mathbf{I}(\mathbf{q})$ is the moment of inertia that depends on the vibrational coordinate q_k, and p_k is the conjugate momentum to q_k. The indices k and k' range over $k = 1, 2, \ldots, 3N-6$, where N is the number of atoms in the system. The coordinate q_k is taken as the normal mode coordinate at the saddle point so that the potential energy $V(\mathbf{q})$ can be expanded as

$$V(\mathbf{q}) = -\frac{\lambda^2}{2}{q_1}^2 + \sum_{k=2}^{f} \frac{{\omega_k}^2}{2}{q_k}^2 + \sum_{\mathbf{j}} c_{\mathbf{j}} {q_1}^{j_1} \ldots {q_f}^{j_f}, \tag{3}$$

where $f \overset{\text{def}}{=} 3N-6$, the coefficients λ^2 and ω_k^2 denote the curvature along the reactive normal mode coordinate q_1 and that along the nonreactive one q_k, respectively. The coefficients $c_{\mathbf{j}}$ describe the strength of anharmonicity of ${q_1}^{j_1}{q_2}^{j_2}\ldots{q_f}^{j_f}$ where $|\mathbf{j}|(\overset{\text{def}}{=}\sum_{k=1}^{f} j_k) \geq 3$. The molecular axes are taken so that the matrix $\mathbf{M}(\mathbf{q})$ is diagonal at the equilibrium point $\mathbf{q} = \mathbf{0}$:

$$\mathbf{M}|_{\mathbf{q}=\mathbf{0}} = 2\begin{pmatrix} A & 0 & 0 \\ 0 & B & 0 \\ 0 & 0 & C \end{pmatrix}, \tag{4}$$

where A, B, and C are called rotational constants. It is a convention in molecular spectroscopy to take the molecular axes so that the rotational constants are in the order $A \geq B \geq C$.[61,62]

The vectors $\boldsymbol{\zeta}_{k,k'}$ represent the Coriolis interaction.

The equation of motion can be derived from the Hamiltonian of Eq. (1) by

$$\frac{\mathrm{d}}{\mathrm{d}t}\phi = \{\phi, H\}, \tag{5}$$

where ϕ may be any physical quantities such as q_k, p_k, or $\mathbf{J}$. The Poisson bracket relations are given by

$$\begin{aligned} \{q_k, p_m\} &= \delta_{km}, \\ \{J_a, J_b\} &= -J_c, \\ \{J_b, J_c\} &= -J_a, \\ \{J_c, J_a\} &= -J_b, \\ \{J_j, q_k\} &= \{J_j, p_k\} = 0, \quad (j = a, b, c), \end{aligned} \tag{6}$$

where δ denotes Kronecker's delta.

B. Rigid rotor and harmonic approximation

Let us start the investigation of the dynamics by the rigid-rotor-harmonic-oscillator approximation, where we ignore the dependence of $\mathbf{M}$ on the vibrational coordinates q_k and the anharmonicities in the potential $V(\mathbf{q})$:

$$H \approx A{J_a}^2 + B{J_b}^2 + C{J_c}^2 + \frac{1}{2}\left({p_1}^2 - \lambda^2{q_1}^2\right) + \frac{1}{2}\sum_{k=2}^{f}\left({p_k}^2 + {\omega_k}^2{q_k}^2\right). \tag{7}$$

Under this Hamiltonian, the vibrational action

$$I_k \overset{\text{def}}{=} \frac{1}{2\omega_k}\left({p_k}^2 + {\omega_k}^2{q_k}^2\right), \quad (k = 2, \ldots, f), \tag{8}$$

the reactive-mode action

$$I_1 \overset{\text{def}}{=} \frac{1}{2\lambda}\left({p_1}^2 - \lambda^2{q_1}^2\right), \tag{9}$$

the total angular momentum

$$|\mathbf{J}|^2 = {J_a}^2 + {J_b}^2 + {J_c}^2, \tag{10}$$

and the rotational energy

$$E_{\mathrm{rot}} \overset{\text{def}}{=} A{J_a}^2 + B{J_b}^2 + C{J_c}^2, \tag{11}$$

are all constants of motion. The phase space structure is depicted in Fig. 1. The trajectories run along the contour curves of the constants of Eqs. (8)–(11), and all the modes are independent of each other, with the whole phase space given by the direct product of these 2D plots.

It is convenient in later calculations to introduce the following variables:

$$\begin{aligned} J_\pm &= J_b \pm \mathrm{i}J_c, \\ x_1 &= \frac{p_1 + \lambda q_1}{\sqrt{2\lambda}}, \quad \xi_1 = \frac{p_1 - \lambda q_1}{\sqrt{2\lambda}}, \\ x_k &= \frac{\omega_k q_k - \mathrm{i}p_k}{\sqrt{2\omega_k}}, \quad \xi_k = \frac{p_k - \mathrm{i}\omega_k q_k}{\sqrt{2\omega_k}}, \quad (k = 2, \ldots, f), \end{aligned} \tag{12}$$

in which the Poisson bracket relations are

$$\begin{aligned} \{J_a, J_\pm\} &= \pm\mathrm{i}J_\pm, \\ \{J_\pm, J_\mp\} &= \pm 2\mathrm{i}J_a, \\ \{x_k, \xi_m\} &= \delta_{km}, \quad (k, m = 1, \ldots, f), \end{aligned} \tag{13}$$

Downloaded 22 Mar 2011 to 133.87.26.199. Redistribution subject to AIP license or copyright; see http://jcp.aip.org/about/rights_and_permissions

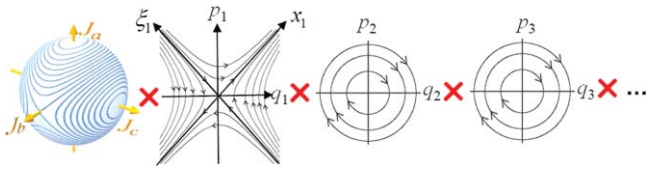

FIG. 1. Phase space flow under the rigid-rotor-harmonic-oscillator approximation. In the **J**-space (left panel), the contour curves of the rotational energy are depicted on the sphere of constant $|\mathbf{J}|$. In the (q_k, p_k)-spaces, the contour curves of the actions are depicted. In all the panels, the trajectories run along these contour curves.

and the action variables [Eqs. (8) and (9)] are

$$I_1 = x_1\xi_1,$$
$$I_k = \mathrm{i}x_k\xi_k, \quad (k = 2, \ldots, f). \tag{14}$$

The most important in the reaction theory is the reaction mode (q_1, p_1). Suppose $q_1 = -\infty$ corresponds to the "reactant" (i.e., before the reaction), and $q_1 = +\infty$ to the "product" (after the reaction). The trajectories with $x_1 > 0$ and $\xi_1 > 0$ are "forward reactive" trajectories because they start in the reactant region, overcomes the barrier, and goes into the product region (in other words, "the reaction occurs"). On the other hand, the trajectories with $x_1 < 0$ and $\xi_1 > 0$ are "forward nonreactive" trajectories because they start in the reactant region, but are reflected by the barrier, and goes back into the reactant region. The trajectories with $x_1 < 0$ and $\xi_1 < 0$ are "backward reactive" trajectories, because they start in the product region and go into the reactant region (the backward reaction). Similarly, the trajectories with $x_1 > 0$ and $\xi_1 < 0$ are "backward nonreactive" trajectories. Note that the sign of the action $I_1 = x_1\xi_1$ determines the reactivity of the trajectory. If $I_1 > 0$, it is reactive (forward or backward). If $I_1 < 0$, it is nonreactive.

The set of all the points with $x_1 = 0$, $|\mathbf{J}| = J$, and $H = E$

$$\mathcal{W}^{\mathrm{s}} \stackrel{\mathrm{def}}{=} \{(\mathbf{J}, \mathbf{x}, \boldsymbol{\xi}) \,|x_1 = 0, |\mathbf{J}| = J, H = E\} \tag{15}$$

is called stable invariant manifold. All points on $\mathcal{W}^{\mathrm{s}}$ remain on $\mathcal{W}^{\mathrm{s}}$ without going either to the reactant or the product regions. All points with $x_1 > 0$ ($x_1 < 0$) go into the product (reactant) region as $t \to +\infty$. Therefore, the manifold $\mathcal{W}^{\mathrm{s}}$ serves as an impenetrable barrier to separate the reactive and the nonreactive trajectories. In other words, it *divides the future* of the trajectory. Likewise, the set

$$\mathcal{W}^{\mathrm{u}} \stackrel{\mathrm{def}}{=} \{(\mathbf{J}, \mathbf{x}, \boldsymbol{\xi}) \,|\xi_1 = 0, |\mathbf{J}| = J, H = E\} \tag{16}$$

is called unstable invariant manifold. All points on $\mathcal{W}^{\mathrm{u}}$ remain on $\mathcal{W}^{\mathrm{u}}$. All points with $\xi_1 > 0$ ($\xi_1 < 0$) came from the reactant (product) region in $t \to -\infty$. Thus the manifold $\mathcal{W}^{\mathrm{u}}$ serves as an impenetrable barrier which *divides the past* of the trajectory. The surface given by

$$\mathcal{T} \stackrel{\mathrm{def}}{=} \{(\mathbf{J}, \mathbf{x}, \boldsymbol{\xi}) \,|q_1 = 0, |\mathbf{J}| = J, H = E\} \tag{17}$$

is called TS. Once a forward-going trajectory crosses the TS, it must go straightforward into the product region, without ever returning into the reactant region before being captured in the product. Thus the TS can be regarded as no-return dividing surface between the reactant and the product regions. Note that the definition of no-return dividing surface is not unique, that is, not restricted to that given by Eq. (17). For instance, the no-return property holds in the definition of the TS in Eq. (17) even if the line $q_1 = 0$ is rotated around the origin in the space of (q_1, p_1) until it hits either of the lines $x_1 = 0$ and $\xi_1 = 0$. On the other hand, the stable manifold $\mathcal{W}^{\mathrm{s}}$ and the unstable manifold $\mathcal{W}^{\mathrm{u}}$ are uniquely determined.

Note that the TS and the stable and the unstable manifolds have the common "anchor" (or boundary). It is given by

$$\mathcal{M} \stackrel{\mathrm{def}}{=} \{(\mathbf{J}, \mathbf{x}, \boldsymbol{\xi}) \,|x_1 = \xi_1 = 0, |\mathbf{J}| = J, H = E\}, \tag{18}$$

and is called NHIM. All points on $\mathcal{M}$ remain on $\mathcal{M}$ for all time. The manifold $\mathcal{M}$ consists of points that remain over the top of the barrier without going either to the reactant or the product region. Note that all points in the stable (unstable) invariant manifold $\mathcal{W}^{\mathrm{s}}$ ($\mathcal{W}^{\mathrm{u}}$) asymptotically approach $\mathcal{M}$ in $t \to \infty$ ($t \to -\infty$). While the definition of TS is not unique, the anchor of the TS must be the NHIM in order to satisfy the nonrecrossing property.

The phase space structure of the rotational mode (left part of Fig. 1)[63,64] is obtained from the conservation of the total angular momentum ($|\mathbf{J}| = $ const., a sphere in the **J**-space), and the conservation of the rotational energy $E_{\mathrm{rot}} = AJ_a{}^2 + BJ_b{}^2 + CJ_c{}^2$ for the asymmetric top $A \geq B \geq C$. In the figure, the contours of E_{rot} are depicted on the sphere of constant $|\mathbf{J}|$. We have four stable fixed points: $J_a = \pm J$, $J_b = J_c = 0$ where E_{rot} is maximum, and $J_a = J_b = 0$, $J_c = \pm J$ where E_{rot} is minimum. The points $J_a = J_c = 0$, $J_b = \pm J$ are also fixed points but they are unstable.

For the case of symmetric top the phase space structure becomes simpler. For the prolate symmetric top, where $A > B = C$, we have $E_{\mathrm{rot}} = B|\mathbf{J}|^2 + (A - B)J_a{}^2$ and the trajectories run along the contour curves of J_a as in Fig. 2(a). For the oblate symmetric top, where $A = B > C$, we have $E_{\mathrm{rot}} = B|\mathbf{J}|^2 - (B - C)J_c{}^2$ and the trajectories run along the contour curves of J_c as in Fig. 2(b). For both prolate and oblate symmetric top cases, there exist two stable fixed points. For the spherical symmetric top case $A = B = C$, all the points in the **J**-space are fixed points, and all the points on the constant-$|\mathbf{J}|$ sphere have the same energy.

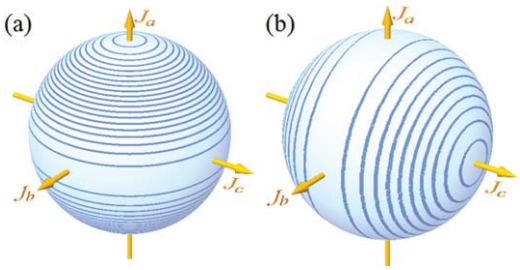

FIG. 2. Phase space flow of the rotational mode drawn for the cases of (a) prolate symmetric top, and (b) oblate symmetric top.

Downloaded 22 Mar 2011 to 133.87.26.199. Redistribution subject to AIP license or copyright; see http://jcp.aip.org/about/rights_and_permissions

C. Normal form theory with spatial rotation

Next we consider the general case [Eq. (1)] with rovibrational couplings and anharmonicity. The idea is similar to the previous studies for the rotationless case.[9,10,17,19,22–39,41,47–51] We introduce a special coordinate transformation $(\mathbf{J}, \mathbf{x}, \boldsymbol{\xi}) \mapsto (\bar{\mathbf{J}}, \bar{\mathbf{x}}, \bar{\boldsymbol{\xi}})$ with which the Hamiltonian is reduced to

$$H = \bar{H}(\bar{\mathbf{J}}, \bar{I}_1, \bar{I}_2, \ldots), \tag{19}$$

that is, the Hamiltonian depends on $(\bar{x}_k, \bar{\xi}_k)$ only through the action variables $\bar{I}_k$ defined by

$$\bar{I}_1 \overset{\text{def.}}{=} \bar{x}_1 \bar{\xi}_1, \quad \bar{I}_k \overset{\text{def.}}{=} \mathrm{i}\bar{x}_k \bar{\xi}_k, \quad (k = 2, \ldots, f), \tag{20}$$

while we allow any functional form with respect to $\bar{\mathbf{J}}$. With this form of the Hamiltonian, it can be shown that the action variables $\bar{I}_k$ are constants of motion. We can therefore draw the same picture as Fig. 1 with the names of the axes replaced by the new variables. The fate of the reaction can be determined solely by the sign of $\bar{x}_1$ at any instant.

We divide the Hamiltonian

$$H = H_0 + H_1 + H_2 + \cdots, \tag{21}$$

as

$$\begin{aligned}
H_0 &= \frac{B+C}{2}|\mathbf{J}|^2 + \left(A - \frac{B+C}{2}\right) {J_a}^2 + \frac{1}{2}\left({p_1}^2 - \lambda^2 {q_1}^2\right) \\
&\quad + \frac{1}{2}\sum_{k=2}^{f}\left({p_k}^2 + {\omega_k}^2 {q_k}^2\right), \\
H_1 &= \frac{B-C}{2}\left({J_b}^2 - {J_c}^2\right) + \frac{1}{2}\sum_k \mathbf{J}^{\mathrm{T}}\mathbf{M}_k^{(1)}\mathbf{J}q_k \\
&\quad - \sum_{k,k'} \boldsymbol{\zeta}_{k,k'}^{\mathrm{T}} q_k p_{k'} \mathbf{M}^{(0)}\mathbf{J} + \sum_{k,k',k''} \alpha_{kk'k''} q_k q_{k'} q_{k''}, \\
H_2 &= \frac{1}{2}\sum_{k,k'} \mathbf{J}^{\mathrm{T}}\mathbf{M}_{k,k'}^{(2)}\mathbf{J}q_k q_{k'} - \sum_{k,k',k''} \boldsymbol{\zeta}_{k,k'}^{\mathrm{T}}\mathbf{M}_{k''}^{(1)}\mathbf{J}q_k p_{k'} q_{k''} \\
&\quad + \frac{1}{2}\sum_{k,k',k'',k'''} \boldsymbol{\zeta}_{k,k'}^{\mathrm{T}}\mathbf{M}^{(0)}\boldsymbol{\zeta}_{k'',k'''} q_k p_{k'} q_{k''} p_{k'''} \\
&\quad + \sum_{k,k',k'',k'''} \alpha_{kk'k''k'''} q_k q_{k'} q_{k''} q_{k'''},
\end{aligned} \tag{22}$$

where we have used the Taylor expansions of the matrix $\mathbf{M}$ and the potential V:

$$\begin{aligned}
\mathbf{M}(\mathbf{q}) &= \mathbf{M}^{(0)} + \sum_k \mathbf{M}_k^{(1)} q_k + \sum_{k,k'} \mathbf{M}_{k,k'}^{(2)} q_k q_{k'} + \cdots, \\
\mathbf{M}^{(0)} &= 2\begin{pmatrix} A & 0 & 0 \\ 0 & B & 0 \\ 0 & 0 & C \end{pmatrix}, \\
V(\mathbf{q}) &= -\frac{\lambda^2}{2}{q_1}^2 + \sum_{k=2}^{f}\frac{{\omega_k}^2}{2}{q_k}^2 + \sum_{k,k',k''} \alpha_{kk'k''} q_k q_{k'} q_{k''} \\
&\quad + \sum_{k,k',k'',k'''} \alpha_{kk'k''k'''} q_k q_{k'} q_{k''} q_{k'''} + \cdots.
\end{aligned} \tag{23}$$

Thus the zeroth order Hamiltonian H_0 consists of the prolate symmetric top and the harmonic approximation. The first-order H_1 contains the deviation from the symmetric top, the rovibrational coupling cubic in $\mathbf{J}$ and $\mathbf{q}$, and the anharmonicity cubic in $\mathbf{q}$. The second order H_2 contains the terms that are quartic in $\mathbf{J}$ and $\mathbf{q}$. Similarly, the higher order parts H_ν $(\nu = 3, 4, \ldots)$ are polynomials of degree $\nu + 2$ in $\mathbf{J}$ and $\mathbf{q}$.

We introduce a formal parameter ε of perturbation, which we set $\varepsilon = 1$ after all the following calculation is done. The Hamiltonian is written as

$$H = H^{(0)} = \sum_{\nu=0}^{\infty} \varepsilon^\nu H_\nu^{(0)}, \tag{24}$$

with $H_\nu^{(0)} = H_\nu$ defined in Eq. (22).

We construct the NF transformation from $(\mathbf{J}, \mathbf{x}, \boldsymbol{\xi})$ to $(\bar{\mathbf{J}}, \bar{\mathbf{x}}, \bar{\boldsymbol{\xi}})$ by Lie canonical perturbation theory.[65] Following the formulation by Dragt and Finn,[66] we perform successive operations of Lie transformations:

$$\begin{aligned}
\bar{J}_i &= \exp(-\varepsilon \mathrm{ad}_{F_1}) \exp(-\varepsilon^2 \mathrm{ad}_{F_2}) \ \ldots \exp(-\varepsilon^m \mathrm{ad}_{F_m}) J_i, \\
\bar{x}_k &= \exp(-\varepsilon \mathrm{ad}_{F_1}) \exp(-\varepsilon^2 \mathrm{ad}_{F_2}) \ \ldots \exp(-\varepsilon^m \mathrm{ad}_{F_m}) x_k, \\
\bar{\xi}_k &= \exp(-\varepsilon \mathrm{ad}_{F_1}) \exp(-\varepsilon^2 \mathrm{ad}_{F_2}) \ \ldots \exp(-\varepsilon^m \mathrm{ad}_{F_m}) \xi_k,
\end{aligned} \tag{25}$$

where m is the order of perturbation and ad_{F_ν} $(\nu = 1, \ldots, m)$ is an operation of Poisson bracket with a function F_ν:

$$\mathrm{ad}_{F_\nu} = \{\cdot, F_\nu\}. \tag{26}$$

The transformation of the Hamiltonian $H(\mathbf{J}, \mathbf{x}, \boldsymbol{\xi}) \mapsto \bar{H}(\bar{\mathbf{J}}, \bar{\mathbf{x}}, \bar{\boldsymbol{\xi}})$ is then given by

$$\bar{H} = \exp(\varepsilon^m \mathrm{ad}_{F_m}) \ \ldots \exp(\varepsilon^2 \mathrm{ad}_{F_2}) \exp(\varepsilon \mathrm{ad}_{F_1}) H. \tag{27}$$

If we define $\bar{H}^{(\mu)}$ and $\bar{H}_\nu^{(\mu)}$ by

$$\begin{aligned}
\bar{H}^{(\mu)} &= \exp(\varepsilon^\mu \mathrm{ad}_{F_\mu}) \bar{H}^{(\mu-1)} \\
&= \exp(\varepsilon^\mu \mathrm{ad}_{F_\mu}) \ \ldots \exp(\varepsilon \mathrm{ad}_{F_1}) H,
\end{aligned} \tag{28}$$

$$\bar{H}^{(\mu)} = \sum_{\nu=0}^{\infty} \varepsilon^\nu \bar{H}_\nu^{(\mu)}, \tag{29}$$

we obtain the following recursion formulas for $\bar{H}_\nu^{(\mu)}$

$$\nu < \mu \ : \ \bar{H}_\nu^{(\mu)} = \bar{H}_\nu^{(\mu-1)}, \tag{30}$$

$$\nu = \mu \ : \ \bar{H}_\mu^{(\mu)} = \bar{H}_\mu^{(\mu-1)} + \{H_0, F_\mu\}, \tag{31}$$

$$\nu > \mu \ : \ \bar{H}_\nu^{(\mu)} = \bar{H}_\nu^{(\mu-1)} + \sum_{s=1}^{\infty} \frac{\left(\mathrm{ad}_{F_\mu}\right)^s}{s!} \bar{H}_{\nu-s\mu}^{(\mu-1)}. \tag{32}$$

In the new Hamiltonian $\bar{H} = \bar{H}^{(m)} = \sum_{\nu=0}^{\infty} \varepsilon^\nu \bar{H}_\nu^{(m)}$, the terms of order ν are

$$\bar{H}_\nu^{(m)} = \bar{H}_\nu^{(m-1)} = \cdots = \bar{H}_\nu^{(\nu)} = \bar{H}_\nu^{(\nu-1)} + \{H_0, F_\nu\}, \tag{33}$$

because of Eqs. (30) and (31). In the above equation, $\bar{H}_\nu^{(\nu-1)}$ is given from the calculations in lower orders. The term $\bar{H}_\nu^{(m)}$ in the new Hamiltonian can be made into a "desirable" form, more precisely the form of Eq. (19), by setting F_ν appropriately.

Downloaded 22 Mar 2011 to 133.87.26.199. Redistribution subject to AIP license or copyright; see http://jcp.aip.org/about/rights_and_permissions

We can express $\bar{H}_\mu^{(\mu-1)}$ and the generating function F_μ as polynomials of $J_\pm, \mathbf{x}, \boldsymbol{\xi}$ defined in Eq. (12)

$$\bar{H}_\mu^{(\mu-1)}(\mathbf{J},\mathbf{x},\boldsymbol{\xi}) = \sum_{\mathbf{j},\mathbf{k}} h_{\mathbf{jk}}^{(\mu-1)}(J_a) J_+^{j_0} J_-^{k_0} x_1^{j_1} \dots x_f^{j_f} \xi_1^{k_1} \dots \xi_f^{k_f},$$

$$F_\mu(\mathbf{J},\mathbf{x},\boldsymbol{\xi}) = \sum_{\mathbf{j},\mathbf{k}} f_{\mathbf{jk}}^{(\mu-1)}(J_a) J_+^{j_0} J_-^{k_0} x_1^{j_1} \dots x_f^{j_f} \xi_1^{k_1} \dots \xi_f^{k_f}. \tag{34}$$

with the coefficients $h_{\mathbf{jk}}^{(\mu-1)}(J_a)$ and $f_{\mathbf{jk}}^{(\mu-1)}(J_a)$ being functions of J_a. Here we must allow a general functional form with respect to J_a, $h_{\mathbf{jk}}^{(\mu-1)}(J_a)$, and $f_{\mathbf{jk}}^{(\mu-1)}(J_a)$, rather than polynomials because we will encounter a division by a polynomial of J_a in the generating function [Eq. (37)], which then goes into the Hamiltonian in the next iteration step. Since we have

$$H_0 = \frac{B+C}{2}|\mathbf{J}|^2 + DJ_a^2 + \lambda x_1 \xi_1 + \sum_k \mathrm{i}\omega_k x_k \xi_k, \tag{35}$$

with $D \overset{\text{def}}{=} A - (B+C)/2$, the Poisson bracket of H_0 and F_μ can be calculated by using Eq. (13):

$$\{H_0, F_\mu\} = \sum_{\mathbf{j},\mathbf{k}} f_{\mathbf{jk}}^{(\mu-1)}(J_a) \gamma_{\mathbf{jk}} J_+^{j_0} J_-^{k_0} x_1^{j_1} \dots x_f^{j_f} \xi_1^{k_1} \dots \xi_f^{k_f},$$

$$\gamma_{\mathbf{jk}} \overset{\text{def}}{=} -2\mathrm{i}D(k_0 - j_0)J_a + \lambda(k_1 - j_1) + \mathrm{i}\sum_{\ell=2}^{f} \omega_\ell (k_\ell - j_\ell). \tag{36}$$

Thus by setting

$$f_{\mathbf{jk}}^{(\mu-1)}(J_a) = -\frac{h_{\mathbf{jk}}^{(\mu-1)}(J_a)}{\gamma_{\mathbf{jk}}} = \frac{-h_{\mathbf{jk}}^{(\mu-1)}(J_a)}{-2\mathrm{i}D(k_0 - j_0)J_a + \lambda(k_1 - j_1) + \mathrm{i}\sum_{\ell=2}^{f} \omega_\ell (k_\ell - j_\ell)}, \tag{37}$$

we can cancel out the terms with the powers $\mathbf{j}, \mathbf{k}$ from the new Hamiltonian.

Canceling the terms with different powers of x_ℓ and ξ_ℓ and leaving those with $j_\ell = k_\ell$ ($\ell = 1, 2, \dots, f$), we obtain the desired result of Eq. (19). (This procedure has been sometimes referred to as *normalization.*) Note that, because we allow any powers of (j_0, k_0) in $\bar{H}$, the variable $\bar{J}_a$ is not a constant of motion, in contrast to the symmetric top case (because $\{J_a, J_+^j J_-^k\} \neq 0$ for $j \neq k$).

It was found in the previous papers[9,10,17,19,22–39,41,47–51,67,68] that the cancellation of the terms with $j_1 \neq k_1$ is possible for any value of λ, and ω_ℓ, because the real part of the denominator $\gamma_{\mathbf{jk}}$ consists of only $\lambda(k_1 - j_1)$, and $\gamma_{\mathbf{jk}}$ is therefore always nonzero for $j_1 \neq k_1$. Here we find that this is also the case even with the existence of the rotation, because the term $-2\mathrm{i}D(k_0 - j_0)J_a$ in Eq. (37) is purely imaginary. On the other hand, the nonreactive modes and the rotational modes may suffer from the problem of small denominator[69] when ω_ℓ's and $2DJ_a$ are in resonance. Note that the resonance condition now depends on the dynamical variable J_a. Whereas H_0 is taken as a symmetric top, the variable J_a is no longer a constant of motion when $H_1, H_2, \dots$ exist. In general, the form $\bar{H}(\bar{\mathbf{J}}, \bar{I}_1, \bar{I}_2, \dots)$ of the new Hamiltonian can cause divergence when nonlinear resonance is met along the time propagation of the dynamics obeying the original Hamiltonian H. The problem of resonance can be avoided by adopting the form $\bar{H}(\bar{\mathbf{J}}, \bar{I}_1, \bar{x}_2, \bar{\xi}_2, \dots)$, that is, we eliminate only the terms with $j_1 \neq k_1$ by Eq. (37) and leave the other terms (which may experience nonlinear resonance) unnormalized. This is called partial normal form and has better convergence property of $\bar{H}$.[19,70,71] Further relaxation of the normalization is also possible, by which we can still extract the stable/unstable invariant manifolds ($\mathcal{W}^{\mathrm{s}}/\mathcal{W}^{\mathrm{u}}$) with yet better convergence even when no-return TS ($\mathcal{T}$) may not exist.[30,49]

Note also that the generating function, and therefore also the new Hamiltonian, are rational functions, rather than polynomials, of the dynamical variable J_a as in Eq. (37). We therefore need manipulations of rational functions in the NF calculations to include the effects of spatial rotation. In the technical aspect, this is the largest difference from the previous papers of NF.

After constructing the transformation $(J_a, J_+, J_-, \mathbf{x}, \boldsymbol{\xi}) \mapsto (\bar{J}_a, \bar{J}_+, \bar{J}_-, \bar{\mathbf{x}}, \bar{\boldsymbol{\xi}})$ in the above procedure, we can introduce real-valued normal form coordinates by

$$\bar{J}_b = (\bar{J}_+ + \bar{J}_-)/2, \quad \bar{J}_c = (\bar{J}_+ - \bar{J}_-)/(2\mathrm{i}),$$
$$\bar{q}_1 = \frac{1}{\sqrt{2\lambda}}(\bar{x}_1 - \bar{\xi}_1), \quad \bar{p}_1 = \sqrt{\frac{\lambda}{2}}(\bar{x}_1 + \bar{\xi}_1),$$
$$\bar{q}_k = \frac{1}{\sqrt{2\omega_k}}(\bar{x}_k + \mathrm{i}\bar{\xi}_1), \quad \bar{p}_k = \sqrt{\frac{\omega_k}{2}}(\bar{\xi}_k + \mathrm{i}\bar{x}_k), \tag{38}$$

similarly to Eq. (12). There is a symmetry property satisfied by the variables, which can be useful for the check of the calculation results. Since there is no external field, the system has a time-reversal symmetry. Thus the Hamiltonian H does not change under the transformation $(\mathbf{J}, \mathbf{q}, \mathbf{p}) \mapsto (-\mathbf{J}, \mathbf{q}, -\mathbf{p})$. The same property must hold after the transformation: $\bar{H}$ does not change under $(\bar{\mathbf{J}}, \bar{\mathbf{q}}, \bar{\mathbf{p}}) \mapsto (-\bar{\mathbf{J}}, \bar{\mathbf{q}}, -\bar{\mathbf{p}})$. Thus in the polynomial expression of $\bar{H}$, the coefficients of even (odd) total power of $\bar{J}_b, \bar{J}_c$, and $\bar{\mathbf{p}}$ must be an even (odd) function of $\bar{J}_a$, respectively. Likewise, in the expression of $\bar{\mathbf{q}}$ in terms of the original variables, the coefficients of even (odd) total power of J_b, J_c, and $\mathbf{p}$ must be an even (odd) function of J_a, respectively. In contrast, in the expression of $\bar{\mathbf{J}}$ and $\bar{\mathbf{p}}$ in terms of the original variables, the coefficients of even (odd) total power of J_b, J_c, and $\mathbf{p}$ must be an odd (even) function of J_a, respectively. (See also the electronic database[72] of the transformed Hamiltonian $\bar{H}$ and transformed physical quantities $\bar{\mathbf{q}}, \bar{\mathbf{J}}$, and $\bar{\mathbf{p}}$ represented in terms of the original variables.)

In the present paper we chose the prolate symmetric top and the harmonic approximation of vibrational degrees of freedom as the zeroth order Hamiltonian. One may replace the prolate symmetric top by the oblate symmetric top as the zeroth order. Then the calculations above can proceed similarly with appropriate change of indices. However, choosing the asymmetric top and the harmonic approximation as the zeroth order would require more complicated calculations.[59] This is because we will encounter Eq. (33), where the

Downloaded 22 Mar 2011 to 133.87.26.199. Redistribution subject to AIP license or copyright; see http://jcp.aip.org/about/rights_and_permissions

Poisson bracket of H_0 with the generating function of the transformation is required to cancel with higher order parts of the Hamiltonian. Solving this equation for the generating function needs an analytical solution for the time evolution obeying H_0. While the analytical solution for the prolate and oblate symmetric tops is given by simple trigonometric functions, that of the asymmetric top involves elliptic functions,[59,64] which would make the calculation more complicated. The resonance condition would also be complicated because the angular frequency of the zeroth order periodic motion in the **J**-space, given by $2DJ_a$ in the prolate case [see Eqs. (35) and (36)], is given for the asymmetric top case by an elliptic function[59,64] with the rotational energy, which in turn is a function of the three components of **J**. In the future, it would be interesting to also develop a normal form theory with the zeroth order being the asymmetric top based on the action-angle expression derived in the Appendix of Ref. 59. At end, the validity of the choice of the zeroth part and the order assignments in the NF calculation should be checked numerically by, for example, comparing the value of the original Hamiltonian and that of the transformed Hamiltonian $\bar{H}$.

III. NUMERICAL EXAMPLE

In this section we demonstrate the calculations by the theory presented in Sec. II with a numerical example of HCN molecule. The molecule undergoes an isomerization between HCN and HNC linear structure:

$$\text{HCN} \rightleftharpoons \text{HNC}. \tag{39}$$

We use the potential surface of Ref. 73. Figure 3 shows the structure, principal axes, and the normal mode vibrations at the saddle point. The mode q_1 is the unstable mode corresponding to HCN $\rightleftharpoons$ HNC isomerization, q_2 is the vibration of the H atom going to and from the CN axis, and q_3 is the stretching vibration of the CN bond. The rotation constants and the normal mode frequencies are

$$A = 14.48\text{cm}^{-1},\quad B = 1.951\ \text{cm}^{-1},\quad C = 1.719\ \text{cm}^{-1},$$
$$\lambda = 1131\ \text{cm}^{-1},\quad \omega_2 = 3129\ \text{cm}^{-1},\quad \omega_3 = 2224\ \text{cm}^{-1}. \tag{40}$$

Since $A > B \approx C$ we take the prolate symmetric top as the zeroth order as in Eq. (22). The calculation is performed up to the second order of perturbation. The original Hamiltonian, the generating functions, the transformed physical quantities $\bar{\mathbf{q}}$, $\bar{\mathbf{J}}$, and $\bar{\mathbf{p}}$, and the transformed Hamiltonian obtained by the NF calculation are given in electronic database.[72]

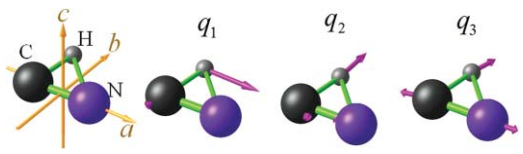

FIG. 3. Structure, principal axes, and normal mode vibrations of HCN molecule at the saddle point.

To grasp the NHIM ($\bar{x}_1 = \bar{\xi}_1 = 0$) obtained by the rotational NF theory, we plot several periodic orbits (POs) within the NHIM. Three POs are chosen where the vibrational mode 2 is excited with $\bar{I}_2 = (3\hbar)/2$, and the mode 3 is kept at the origin $\bar{q}_3 = \bar{p}_3 = 0$. The $\bar{\mathbf{J}}$ is kept at the fixed points in the $\bar{\mathbf{J}}$-space. These points are obtained by solving $\partial \bar{H}(\bar{\mathbf{J}}, \bar{\mathbf{I}})/\partial \bar{\mathbf{J}} = \mathbf{0}$ with the given $\bar{\mathbf{I}}$ and $|\mathbf{J}|$. Table I shows the values of $\bar{\mathbf{J}}$ and the energy ($\bar{H}$) for the chosen POs. The values of $|\mathbf{J}|$ are chosen so that the three POs fall into approximately a similar energy range of ≈1.0 eV. Note that the fixed points in the **J**-space were at $(J_a, J_b, J_c) = (J, 0, 0)$, $(0, J, 0)$, and $(0, 0, J)$ in the rigid rotor approximation (Sec. II B). The locations of the fixed points in the $\bar{\mathbf{J}}$-space deviate from these due to the rovibrational couplings. In this particular example, however, the deviation is small.

The accuracy of the normal form calculation can be assessed by the energy error.[30,70] We compare the value of $\bar{H}$ truncated at μth order perturbation with true Hamiltonian H. The difference is denoted by $\Delta H^{(\mu)}$. The smaller this value is, the better description the normal form Hamiltonian $\bar{H}$ is. Table I shows the mean square of $\Delta H^{(\mu)}$ along each PO for zeroth, first, and second order perturbations. The improvement is appreciable and gets better as the order increases, implying the validity of our rotational NF calculation.

Figure 4(a) shows a periodic orbit in the NF coordinates. In this PO, we excite the vibrational mode 2 with $\bar{I}_2 = (3\hbar)/2$, while keeping the mode 3 at the origin $\bar{q}_3 = \bar{p}_3 = 0$. The rotational mode is kept at the fixed point $\bar{J}_a \approx J$, $\bar{J}_b \approx \bar{J}_c \approx 0$. To capture the relation between the transformed coordinates and more intuitional, naïve coordinates, we next project the periodic orbit onto the (a_H, b_H), the

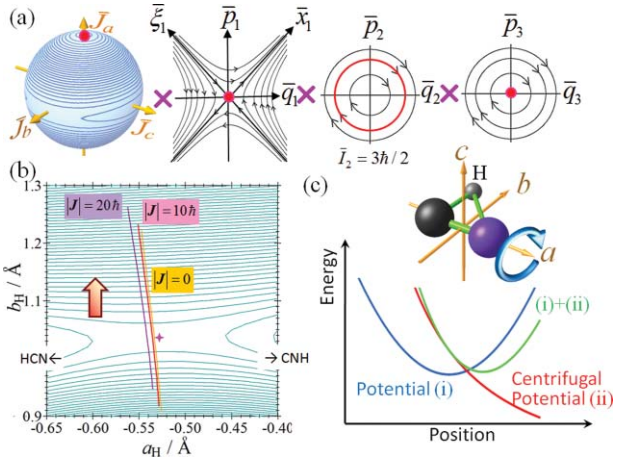

FIG. 4. A periodic orbit in the NHIM ($\bar{x}_1 = \bar{\xi}_1 = 0$). The vibrational mode 2 is excited with $\bar{I}_2 = (3\hbar)/2$, while the mode 3 is kept at the origin $\bar{q}_3 = \bar{p}_3 = 0$. The rotational mode is kept at a fixed point $\bar{J}_b, \bar{J}_c \approx 0$. (a) The phase space diagram in the normal form coordinates. The energy contours in the $\bar{\mathbf{J}}$-space are drawn for $|\mathbf{J}| = 20\,\hbar$ with spacing of 0.02 eV. Big spots in the plots of $\bar{\mathbf{J}}$, $\bar{x}_1$, $\bar{\xi}_1$, $\bar{q}_3$, and $\bar{p}_3$, and the bold circle in $\bar{q}_2$ and $\bar{p}_2$ indicate the position of the chosen periodic orbit. (b) Projection of the periodic orbit onto (a_H, b_H), the position of the H atom in the rotating molecular frame. Contours of the potential energy spaced by 0.02 eV are drawn with the CN distance fixed at the equilibrium. The cross symbol shows the location of the saddle point $(a_\text{H}, b_\text{H}) = (-0.528\text{Å}, 1.037\text{Å})$. (c) A schematic diagram to explain the migration of NHIM with increasing angular momentum $|\mathbf{J}|$. The horizontal axis corresponds approximately to the direction of b_H.

Downloaded 22 Mar 2011 to 133.87.26.199. Redistribution subject to AIP license or copyright; see http://jcp.aip.org/about/rights_and_permissions

TABLE I. Values of the normal form angular momentum $\bar{\mathbf{J}}$, energy $\bar{H}$, and the mean error for the four periodic orbits illustrated in the present paper. The unit of the angular momentum is $\hbar$. The unit of energy is eV.

No.	$\lvert\mathbf{J}\rvert$	$\bar{J}_a$	$\bar{J}_b$	$\bar{J}_c$	$\bar{H}$	$\langle\Delta H^{(0)^2}\rangle^{1/2}$	$\langle\Delta H^{(1)^2}\rangle^{1/2}$	$\langle\Delta H^{(2)^2}\rangle^{1/2}$
1	20	19.9998	−0.0792	0.0000	1.23	0.2461	0.0733	0.0275
2	50	−0.3110	49.9990	0.0000	1.16	0.0800	0.0339	0.0274
3	50	0.0000	0.0000	50.0000	1.09	0.0867	0.0371	0.0311
4	40	...	...	...	1.25	0.0017	0.0018	0.0009

position of the H atom projected onto the molecular inertial axes a and b. In Fig. 4(b), the periodic orbit is superposed on the contour plot of the potential energy surface as functions of (a_{H}, b_{H}). The potential contours are drawn with CN fixed at the equilibrium distance. The position of the saddle point is shown by the cross symbol. The left side corresponds to the HCN structure, and the right to the HNC structure. The periodic orbit is drawn for three different values of $|\mathbf{J}|$: 0, 10 $\hbar$, and 20 $\hbar$. Due to the anharmonicity, the position of the periodic orbit slightly deviates from the saddle point already for $J = 0$. As $\bar{J}_a \approx J$ increases, the orbit migrates toward the upper direction. The qualitative explanation of this upward migration of the PO is given in panel (c). Since we have $\bar{J}_a \approx J$ and $\bar{J}_b \approx \bar{J}_c \approx 0$, the molecule is rotating mostly around the a-axis. Thus the centrifugal force operates in the direction departing from the a-axis, that is, the upward direction along b_{H}. The direction of the centrifugal force is indicated in panel (b) by the arrow. The potential has a minimum along the b_{H}-direction, as seen from the contour plot [Fig. 4(b)] and also from the fact that the b_{H}-direction has the largest projection onto the vibrational normal mode 2 at the saddle point (Fig. 3). When the rotational motion exists, the system feels a centrifugal potential which goes downward in increasing b_{H}. The resulting effective potential is given by the sum of the original potential and the centrifugal one. As illustrated in panel (c), the position of the minimum in the effective potential is found in the direction of lower centrifugal potential. Thus the migration of PO in the same direction as the centrifugal force is qualitatively understood. The PO also migrates in the a_{H}-direction. Since there is no centrifugal force in this direction, this must be due to the anharmonicity of the potential energy surface. The migration of the PO in the b_{H} arising from the centrifugal force also affects its location along a_{H}-direction through the nonlinear coupling between a_{H} and b_{H}.

In the above explanation, we interpreted $\bar{J}_a \approx J$, $\bar{J}_b \approx \bar{J}_c \approx 0$ as rotation around the a-axis. This is only qualitatively true, because $\bar{J}_a$ is a nonlinear function of ($\mathbf{J}$, $\mathbf{q}$, $\mathbf{p}$) through the NF transformation constructed in Sec. II. The motion in $\bar{\mathbf{J}}$ has components in the original $\mathbf{J}$ as well as the internal coordinates ($\mathbf{q}$, $\mathbf{p}$). In other words, it is not a pure rotation. J_a is the "main part" (zeroth order approximation) of $\bar{J}_a$. The above interpretation is therefore qualitatively correct.

Figure 5 shows another periodic orbit in the NHIM. In this case, we have rotational motion around the b-axis ($\bar{J}_b \approx J$, $\bar{J}_a \approx \bar{J}_c \approx 0$), while the vibrational motion is the same as before. This periodic orbit is unstable in the $\bar{\mathbf{J}}$-space as well as in the ($\bar{q}_1$, $\bar{p}_1$)-space. Panel (b) shows the projection of the periodic orbit onto the (a_{H}, b_{H}). It is found that the orbit migrates toward the positive direction along the a_{H}-axis as $\bar{J}_b \approx J$ increases. In this case the molecule rotates around the b-axis, generating the centrifugal force making the hydrogen atom leave from the origin in the a_{H}-direction. When the hydrogen atom is located in a region of negative value of a_{H}, the centrifugal force acts in the negative a_{H} direction [indicated by the arrow in panel (b)]. The migration of the PO with increasing J is in the opposite direction to the centrifugal force, in contrast to the previous case. The a_{H}-direction has the largest projection onto the reaction mode q_1 as seen in Fig. 3. The potential shows a maximum along this direction. As shown schematically in panel (c), the sum of the potential having a maximum and the centrifugal potential exhibits a maximum that is shifted in the direction of *increasing* centrifugal potential.

Figure 6 shows another periodic orbit in the NHIM, with $\bar{J}_c \approx J$, $\bar{J}_a \approx \bar{J}_b \approx 0$, while the vibrational motion is the same as before. This periodic orbit is stable in the $\bar{\mathbf{J}}$-space, and unstable only in the ($\bar{x}_1$, $\bar{\xi}_1$)-space. In this case, the molecule is rotating in the molecular plane (the ab-plane). A marked difference from the previous two cases is that the orbits show circular shapes when projected onto the $a_{\mathrm{H}}b_{\mathrm{H}}$-plane as in panel (b). This is the effect of Coriolis force because the rotation around the c-axis arises the Coriolis force in the ab-plane. The radius of this circular shape of the PO gets larger as $|\mathbf{J}|$ increases, showing the increased effect of the Coriolis force. The location of the PO also changes slightly toward the upper-right as $|\mathbf{J}|$ increases. This can be explained in the same way with the preceding two cases. The centrifugal force generated by the rotation around the c-axis pushes the system from the

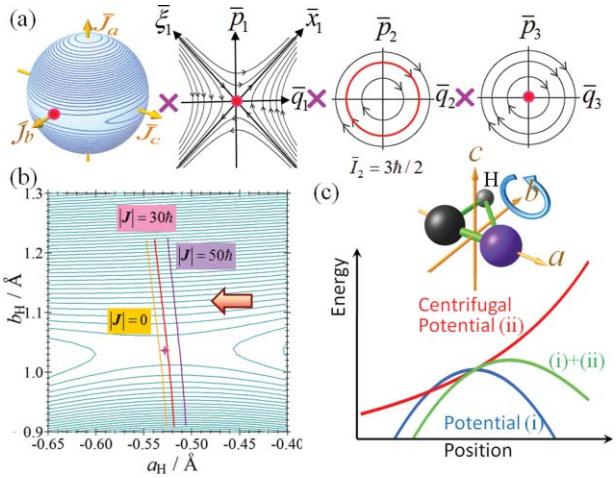

FIG. 5. Same as Fig. 4 except that $\bar{J}_b \approx J$, $\bar{J}_a \approx \bar{J}_c \approx 0$, and the energy contours in the $\bar{\mathbf{J}}$-space are drawn for $|\mathbf{J}| = 50\,\hbar$ with spacing of 0.1 eV. The horizontal axis in (c) corresponds approximately to the direction of a_{H}.

Downloaded 22 Mar 2011 to 133.87.26.199. Redistribution subject to AIP license or copyright; see http://jcp.aip.org/about/rights_and_permissions

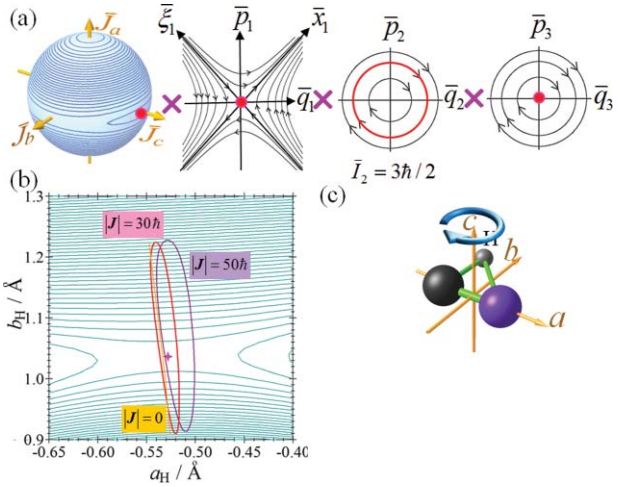

FIG. 6. Same as Fig. 5 except that $\bar{J}_c \approx J$, $\bar{J}_a \approx \bar{J}_b \approx 0$.

origin both in a- and b-directions. The migration of the PO is in the same direction with the centrifugal force along the b_H-direction and in the opposite direction along the a_H-direction, as explained in the preceding paragraphs.

In summary, the three components $(\bar{J}_a, \bar{J}_b, \bar{J}_c)$ of $\bar{\mathbf{J}}$ exhibit different effects on the NHIM. The figures were shown only for the POs in the NHIM by exciting one vibrational mode. When the other mode (q_3) is also excited, we have found that the projection onto the $a_H b_H$-space exhibits Lissajous-type figures winding around the POs shown above (data not shown). The qualitative trend of the migration is the same with the POs: $\bar{J}_a$ shifts the NHIM in the direction of the centrifugal force. $\bar{J}_b$ shifts the NHIM in the direction opposite to the centrifugal force. $\bar{J}_c$ changes the shape of the projection of NHIM on the position space into circular orbits.

Finally, we plot another periodic orbit to show the difference between the transformed angular momentum $\bar{\mathbf{J}}$ and the original one $\mathbf{J}$. In Fig. 7, both the vibrational modes are kept at the origin $\bar{q}_2 = \bar{p}_2 = \bar{q}_3 = \bar{p}_3 = 0$ (see also No. 4 in Table I). An energy contour curve in the $\bar{\mathbf{J}}$-space is taken

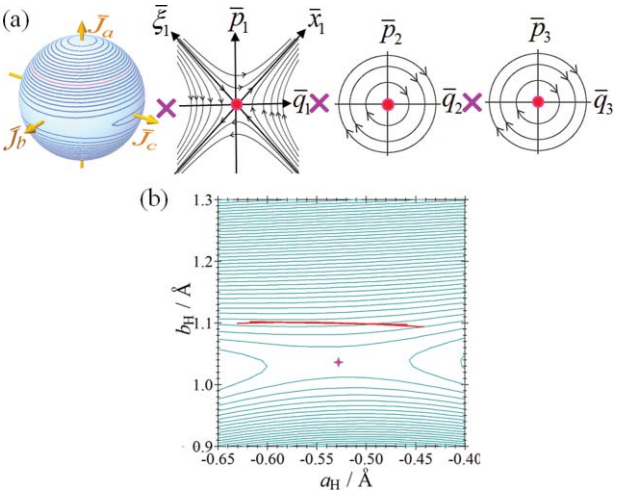

FIG. 7. Same as Fig. 4 except that $\bar{I}_2 = 0$ and a periodic motion in $\bar{\mathbf{J}}$-space is taken. The energy contours in the $\bar{\mathbf{J}}$-space are drawn for $|\mathbf{J}| = 40\,\hbar$ with spacing of 0.1 eV.

to give a periodic orbit. In the projection onto the (a_H, b_H), which is internal coordinates, we see a line segment rather than a point. This means that the periodic motion purely in the $\bar{\mathbf{J}}$ have nonzero projection onto the internal motion of the molecule. Due to the rovibrational coupling, the rotational motion $(\mathbf{J})$ is not independent of the internal (reaction and vibration) motions. In contrast, the normal form coordinate $\bar{\mathbf{J}}$ *is* independent of $(\bar{q}_1, \bar{p}_1, \bar{q}_2, \bar{p}_2, \bar{q}_3, \bar{p}_3)$, since the NF transformation cancels out the couplings. The independent mode $\bar{\mathbf{J}}$ thus constructed is not a pure rotation in the sense of the original coordinate $(\mathbf{J}, \mathbf{q}, \mathbf{p})$ but contains some components in the internal motion. The NF method presented in this study extracts truly separable coordinates in systems under rovibrational couplings. Projecting the NHIM obtained by thus constructed coordinates onto the original coordinate reveals the effects of rovibrational motions on the reaction.

IV. SUMMARY AND OUTLOOK

Recently developed nonlinear dynamical theories of saddle crossings were extended to systems with nonzero spatial rotation. Three components (projection onto the molecular axes) of the angular momentum are not constants of motion (while they are mutually related with each other through the constancy of the modulus of the angular momentum), and were therefore treated as dynamical variables. The rotation is dynamically coupled to the internal motion of the molecule through centrifugal and Coriolis interactions, affecting therefore the reaction process. Under the rovibrational couplings, the method shown in the present paper extracts a new set of coordinates, with which the reaction mode is decoupled from the others. We can thus identify a no-return TS to separate the reactant and the product regions [Eq. (17)], and the stable/unstable invariant manifolds acting as the boundary of reactive and nonreactive trajectories [Eqs. (15) and (16)]. The nonlinear coordinate transformation with spatial rotation requires manipulation of rational functions, in contrast to that without spatial rotation in which only the manipulation of polynomials, easier in the implementation, was needed. The positions of NHIM, which is regarded as an "anchor" of TS, and the stable/unstable invariant manifolds were investigated by projecting several representative periodic orbits in the NHIM back to the original coordinates. It was found that the position of NHIM migrates as the rotation is excited. The three components of the angular momentum were shown to have different effects on the position of NHIM. When the centrifugal force is along the reaction mode, the NHIM migrates in the direction opposite to the centrifugal force. When the centrifugal force is along the vibrational mode, the NHIM migrates in the same direction as the centrifugal force. When the rotation is perpendicular to the internal motion, the Coriolis interaction plays a significant role to make the shape of NHIM circular when projected onto the configuration space.

With the method presented in this paper, the reaction dynamics theory in the nonlinear regime[9,10,17,19,22–38] is now made applicable to a much wider class of realistic systems, such as the bimolecular collision with nonzero impact parameters and the unimolecular reaction with thermally excited rotation. The extraction of the boundary of reaction (that is,

Downloaded 22 Mar 2011 to 133.87.26.199. Redistribution subject to AIP license or copyright; see http://jcp.aip.org/about/rights_and_permissions

stable/unstable invariant manifolds) will progress our insights into what determines the outcome of reactions. An obvious next step is systematic studies of reaction dynamics on precise potential surfaces by highly accurate *ab initio* calculations for the reactions occurring in atmospheric or interstellar regions using the method developed here. It is also interesting that the dynamical structure changes at higher energies.[16,19,30] In contrast to the present treatment, where all the vibrational actions perform as constants of motion by the NF transformation, there should exist a range of energy in which only the action along the reactive coordinate does so while most of all vibrational modes exhibit chaotic motions, or in which even the reactive-mode action is broken but we can still find the reactivity boundary (stable/unstable invariant manifolds).[30,49] The breakdown of the constancy of actions primarily occurs through resonance, that is, a small denominator arises in the generating function for certain combinations of powers and frequencies, causing the divergence of the transformation. It is interesting to note that the denominator depends on the angular momentum [Eq. (37)]. A new type of resonance, therefore a new way of breakdown of dynamical structure, may arise depending on the value of angular momentum. An example of resonance between the rotational and the vibrational motions is the Coriolis resonance,[62,74,75] which corresponds to the case of $j_0 - k_0 = 0, \pm 1$, $j_s - k_s = 1$ and $j_r - k_r = -1$ $(r, s \geq 2, r \neq s)$ in Eq. (37), arising from the terms $\mathbf{J}^{\mathrm{T}}\mathbf{M}(\mathbf{0})\boldsymbol{\zeta}_{rs}q_s p_r$ in Eq. (1). The effect of rovibrational resonance is to generate island chain structures in the **J**-space[58] in place of the simple rigid rotor structure in Sec. II B, or chaotic breakdown of the separatrix and transfer between A-type and C-type rotations.[57,58] It can also change the coupling of vibrational modes[55,56] and exchange energy.[57,58] How the rovibrational resonance affects the *reactive mode* (which is not a vibration) is still to be investigated. Such resonance may mix the rotation and the vibration and increase the phase space dimensionality from $6N - 13$ (purely vibrational) to $6N - 10$ (maximum) as energy increases.[52] These are some of the forthcoming subjects still to be addressed.

ACKNOWLEDGMENTS

This work has been supported by Research Fellowships of the Japan Society for the Promotion of Science for Young Scientists (to S.K.) and by JSPS, JST/CREST, Priority Area "Molecular Theory for Real Systems" (to T.K.). The computations were partially performed using the Research Center for Computational Science, Okazaki, Japan.

[1] H. Eyring, J. Chem. Phys. **3**, 107 (1935).
[2] E. Wigner, J. Chem. Phys. **5**, 720 (1937).
[3] M. G. Evans and M. Polanyi, Trans. Faraday Soc. **31**, 875 (1935).
[4] O. K. Rice and H. C. Ramsperger, J. Am. Chem. Soc. **50**, 617 (1928).
[5] L. S. Kassel, J. Phys. Chem. **32**, 1065 (1928).
[6] R. A. Marcus, J. Chem. Phys. **20**, 359 (1952).
[7] J. C. Keck, Adv. Chem. Phys. **13**, 85 (1967).
[8] D. G. Truhlar and B. C. Garrett, Acc. Chem. Res. **13**, 440 (1980).
[9] *Geometrical Structures of Phase Space in Multidimensional Chaos: Applications to Chemical Reaction Dynamics in Complex Systems* edited by M. Toda, T. Komatsuzaki, T. Konishi, R. S. Berry, and S. A. Rice, Advances in Chemical Physics Vol. 130A and 130B (Wiley, New York, 2005), and references therein.
[10] *Advancing Theory for Kinetics and Dynamics of Complex, Many-Dimensional Systems: Clusters and Proteins*, edited by T. Komatsuzaki, R. S. Berry, and D. M. Leitner, Advances in Chemical Physics, Vol. 145 (Wiley, New York, 2010).
[11] T. Komatsuzaki and R. S. Berry, Adv. Chem. Phys. **123**, 79 (2002).
[12] M. Toda, Adv. Chem. Phys. **123**, 153 (2002).
[13] T. Komatsuzaki and R. S. Berry, Adv. Chem. Phys. **130**, 143 (2005).
[14] M. Toda, Adv. Chem. Phys. **130**, 337 (2005).
[15] C. Jaffé, S. Kawai, J. Palacián, P. Yanguas, and T. Uzer, Adv. Chem. Phys. **130**, 171 (2005).
[16] S. Kawai, H. Teramoto, C.-B. Li, T. Komatsuzaki, and M. Toda, "Dynamical Reaction Theory based on Geometric Structures in Phase Space," Adv. Chem. Phys. (in press).
[17] T. Bartsch, J. M. Moix, R. Hernandez, S. Kawai, and T. Uzer, Adv. Chem. Phys. **140**, 191 (2008).
[18] R. B. Shirts and W. P. Reinhardt, J. Chem. Phys. **77**, 5204 (1982).
[19] C.-B. Li, A. Shojiguchi, M. Toda, and T. Komatsuzaki, Phys. Rev. Lett. **97**, 028302 (2006).
[20] H. Teramoto and T. Komatsuzaki, Phys. Rev. E **78**, 017202 (2008).
[21] H. Teramoto and T. Komatsuzaki, J. Chem. Phys. **129**, 094302 (2008).
[22] S. Kawai, A. D. Bandrauk, C. Jaffé, T. Bartsch, J. Palacián, and T. Uzer, J. Chem. Phys. **126**, 164306 (2007).
[23] T. Komatsuzaki and M. Nagaoka, J. Chem. Phys. **105**, 10838 (1996).
[24] T. Komatsuzaki and M. Nagaoka, Chem. Phys. Lett. **265**, 91 (1997).
[25] H. Waalkens, A. Burbanks, and S. Wiggins, J. Chem. Phys. **121**, 6207 (2004).
[26] C.-B. Li, Y. Matsunaga, M. Toda, and T. Komatsuzaki, J. Chem. Phys. **123**, 184301 (2005).
[27] S. Kawai, Y. Fujimura, O. Kajimoto, T. Yamashita, C.-B. Li, T. Komatsuzaki, and M. Toda, Phys. Rev. A **75**, 022714 (2007).
[28] S. Wiggins, L. Wiesenfeld, C. Jaffé, and T. Uzer, Phys. Rev. Lett. **86**, 5478 (2001).
[29] T. Uzer, C. Jaffé, J. Palacián, P. Yanguas, and S. Wiggins, Nonlinearity **15**, 957 (2002).
[30] S. Kawai and T. Komatsuzaki, Phys. Rev. Lett. **105**, 048304 (2010).
[31] T. Komatsuzaki and R. S. Berry, J. Chem. Phys. **110**, 9160 (1999).
[32] T. Komatsuzaki and R. S. Berry, Phys. Chem. Chem. Phys. **1**, 1387 (1999).
[33] T. Komatsuzaki and R. S. Berry, J. Chem. Phys. **115**, 4105 (2001).
[34] T. Komatsuzaki and R. S. Berry, J. Mol. Struct.: THEOCHEM **506**, 55 (2000).
[35] T. Komatsuzaki and R. S. Berry, Proc. Natl. Acad. Sci. U.S.A. **98**, 7666 (2001).
[36] T. Komatsuzaki and R. S. Berry, J. Phys. Chem. A **106**, 10945 (2002).
[37] W. Koon, M. Lo, J. Marsden, and S. Ross, Chaos **10**, 427 (2000).
[38] C. Jaffe, S. D. Ross, M. W. Lo, J. Marsden, D. Farrelly, and T. Uzer, Phys. Rev. Lett. **89**, 011101 (2002).
[39] H. Waalkens, R. Schubert, and S. Wiggins, Nonlinearity **21**, R1 (2008).
[40] A. Goussev, R. Schubert, H. Waalkens, and S. Wiggins, J. Chem. Phys. **131**, 144103 (2009).
[41] S. Kawai and T. Komatsuzaki, J. Chem. Phys. **134**, 024317 (2011).
[42] T. Bartsch, R. Hernandez, and T. Uzer, Phys. Rev. Lett. **95**, 058301 (2005).
[43] T. Bartsch, T. Uzer, and R. Hernandez, J. Chem. Phys. **123**, 204102 (2005).
[44] T. Bartsch, T. Uzer, J. M. Moix, and R. Hernandez, J. Chem. Phys. **124**, 244310 (2006).
[45] T. Bartsch, J. Chem. Phys. **131**, 124121 (2009).
[46] R. Hernandez, T. Uzer, and T. Bartsch, Chem. Phys. **370**, 270 (2010).
[47] S. Kawai and T. Komatsuzaki, J. Chem. Phys. **131**, 224505 (2009).
[48] S. Kawai and T. Komatsuzaki, J. Chem. Phys. **131**, 224506 (2009).
[49] S. Kawai and T. Komatsuzaki, Phys. Chem. Chem. Phys. **12**, 7626 (2010).
[50] S. Kawai and T. Komatsuzaki, Phys. Chem. Chem. Phys. **12**, 7636 (2010).
[51] S. Kawai and T. Komatsuzaki, Phys. Chem. Chem. Phys. **12**, 15382 (2010).
[52] T. L. Beck, D. M. Leitner, and R. S. Berry, J. Chem. Phys. **89**, 1681 (1988).
[53] L. Wiesenfeld, A. Faure, and T. Johann, J. Phys. B **36**, 1319 (2003).
[54] L. Wiesenfeld, Few-Body Syst. **34**, 163 (2004).
[55] W. B. Clodius and R. B. Shirts, J. Chem. Phys. **81**, 6224 (1984).
[56] T. Uzer, G. A. Natanson, and J. T. Hynes, Chem. Phys. Lett. **122**, 12 (1985).
[57] J. H. Frederick, G. M. McClelland, and P. Brumer, J. Chem. Phys. **83**, 190 (1985).
[58] G. Ezra, Chem. Phys. Lett. **127**, 492 (1986).
[59] J. H. Frederick and G. M. McClelland, J. Chem. Phys. **84**, 4347 (1986).

Downloaded 22 Mar 2011 to 133.87.26.199. Redistribution subject to AIP license or copyright; see http://jcp.aip.org/about/rights_and_permissions

[60]E. B. Wilson, J. C. Decius, and P. C. Cross, *Molecular Vibrations: The Theory of Infrared and Raman Vibrational Spectra* (Dover, New York, 1955).
[61]R. N. Zare, *Angular Momentum* (Wiley, New York, 1988).
[62]P. R. Bunker and P. Jensen, *Molecular Symmetry and Spectroscopy* (National Research Council of Canada, Ottawa, 2006).
[63]H. Goldstein, C. Poole, and J. Safko, *Classical Mechanics*, 3rd ed. (Addison-Wesley, San Francisco, 2002).
[64]L. D. Landau and E. M. Lifshitz, *Mechanics* (Elsevier, Amsterdam, 1976).
[65]A. Deprit, Celest. Mech. **1**, 12 (1969).
[66]A. J. Dragt and J. M. Finn, J. Math. Phys. **20**, 2649 (1979).
[67]R. Hernandez and W. H. Miller, Chem. Phys. Lett. **214**, 129 (1993).
[68]R. Hernandez, J. Chem. Phys. **101**, 9534 (1994).
[69]A. Lichtenberg and M. Lieberman, *Regular and Chaotic Dynamics* (Springer, New York, 1992).
[70]S. Kawai, C. Jaffé, and T. Uzer, J. Phys. B: At. Mol. Opt. Phys. **38**, S261 (2005).
[71]C.-B. Li, A. Shojiguchi, M. Toda, and T. Komatsuzaki, Few-Body Syst. **38**, 173 (2006).
[72]See supplementary material at http://dx.doi.org/10.1063/1.3554906 for the full explicit expressions of the results of NF calculations.
[73]J. N. Murrell and S. Carter, J. Mol. Spectrosc. **93**, 307 (1982).
[74]K.-E. J. Hallin, J. W.C. Johns, and A. Trombetti, Can. J. Phys. **59**, 663 (1981).
[75]F. Hegelund, H. Bürger, and O. Polanz, J. Mol. Spectrosc. **122**, 462 (1987).

Downloaded 22 Mar 2011 to 133.87.26.199. Redistribution subject to AIP license or copyright; see http://jcp.aip.org/about/rights_and_permissions